2014 IEEE International Conference on Robotics & Automation (ICRA)
Hong Kong Convention and Exhibition Center
May 31 - June 7, 2014. Hong Kong, China

Design and Evaluation of Duty-Cycling Steering Algorithms for Robotically-Driven Steerable Needles

Ann Majewicz, Joshua J. Siegel, Andrew A. Stanley, and Allison M. Okamura

***Abstract*— Asymmetric-tip, robotically controlled steerable needles have the potential to improve clinical outcomes for many needle-based procedures by allowing the needle to curve and change direction within biological tissue. Algorithms have previously been developed to change the curvature of the needle trajectory via duty-cycled spinning. However, these algorithms require continuous rotation of the steerable needle, preventing the use of instrumentation such as force-torque sensors and electromagnetic trackers, due cable wind-up issues. In this paper, we present two novel control methods for duty-cycling a steerable needle without the need for continuous rotation: bidirectional duty-cycled spinning and duty-cycled flipping. These algorithms can be implemented on existing robotic needle steering systems without hardware changes. We evaluate our algorithms using a custom hollow steerable needle, with an embedded EM tracker and a force-torque sensor. We compare the path tracking error, needle insertion forces, and needle axial rotation torques of our algorithms and found no significant differences between the two algorithms in terms of tracking error. Duty-cycled flipping has significantly lower mean insertion forces and torques than bidirectional duty-cycled spinning, and differences in insertion force and rotation torque variability were also found. These results may have interesting implications for tissue health.**

I. INTRODUCTION

Robotically steered needles show great promise for improving needle-based medical procedures (e.g. biopsy, ablation, and brachytherapy), as shown by prior demonstrations of needle steering applications in biological tissue [1], [2], [3], [4]. Our needle steering technique exploits asymmetric tip forces to steer needles along constant-curvature paths during insertion [5]. The curvature of the needle path can be controlled in two or three dimensions using duty-cycled spinning algorithms [6], [7].

During duty-cycled spinning, the needle path varies between a maximally curved path (resulting from pure needle insertion) and a minimally curved path (resulting from needle insertion with continuous axial rotation, ideally zero curvature). In duty-cycled spinning, a full needle rotation must be achieved at each duty cycle step to prevent planar deviation of the needle during insertion. Additionally, the rotation (spin) velocity must be much greater than the insertion velocity to prevent helical needle trajectories, though it is possible to exploit these trajectories for needle control [8].

Duty-cycled spinning has been implemented in a variety of needle steering systems [9], [10], [11]. However, the integration of wired sensors with these systems is largely absent from this work, limiting the information can that be gleaned from steerable needle insertion. For example, force sensors are useful for modeling needle-tissue interactions and detecting transitions between tissue types [12]. EM trackers are becoming increasingly popular for detection of the position and orientation of minimally invasive surgical tools such as steerable probes [13], brachytherapy needles [14], and very recently, steerable needles [15], due their small size and accuracy. This is especially important for ultrasound-based procedures, since identifying the needle tip is difficult.

The challenge in using wired sensors with steerable needles is cable wind-up during continuous rotation, which could damage the sensor. It may be possible to avoid this issue with an electrical slip ring; however, this requires hardware changes to the robot design and adds potentially disruptive electromagnetic interference (EMI) from the rotating brushes. Low EMI electrical-optical slip rings exist, but are very expensive. A novel control algorithm could be a simpler, more elegant solution.

In this paper, we present two methods for duty-cycling steerable needles that do not require continuous needle rotation: bidirectional duty-cycled spinning and duty-cycled flipping (Fig. 1). We evaluate these methods using an EM tracker and a force-torque sensor integrated with a novel hollow steerable needle. Additionally, we compare our methods for duty-cycling the needle to the previously developed continuous rotation methods by simulating the expected needle path from encoder readings, and generating ideal needle paths based on theoretical predictions.

As the needle design and duty-cycling algorithms presented in this paper enable the use of sensors with robotically steered needles, our methods could be useful in a variety of

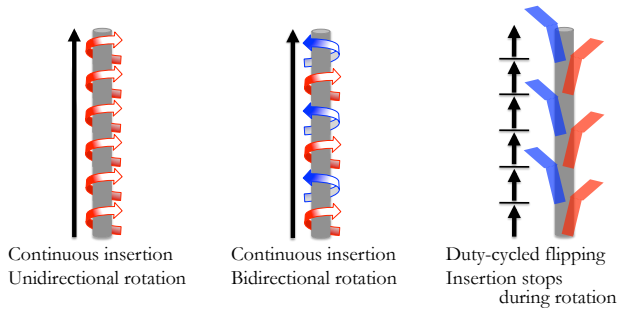

Fig. 1: Needle steering algorithms: continuous duty-cycled spinning (DCS), bidirectional duty-cycled spinning (BDCS), and duty-cycled bevel flipping (DCF).

This work was supported in part by National Science Foundation grants 1217635 and 1227406, a National Science Foundation Graduate Fellowship, and Stanford University.

A. Majewicz, J. J. Siegel, A. A. Stanley, and A. M. Okamura are with the Department of Mechanical Engineering, Stanford University, Stanford, CA 94305, USA, email: Ann.Majewicz@stanford.edu

applications. For example, the EM tracker could provide experimental validation of an almost global estimator for needle pose [16], force and torque measurements could support claims of reduced tissue damage for a novel flexure-based steerable needle [9], and 3D position measurements of the needle tip will enable implementation of a Cartesian-space teleoperation algorithm with a needle steering robot [17]. Additionally, new methods for 3D segmentation of a curved needle using Doppler ultrasound and vibration could also benefit from this work as an electromagnetic tracker would provide a gold standard position measurement in biological tissue [18]. Finally, the discrete nature of our bidirectional duty-cycle flipping method could be useful for a novel discrete-step needle insertion controller [19].

II. Duty-Cycling Algorithms for Variable Needle Curvature

The three methods of duty-cycling a steerable needle evaluated in this work are shown in Fig. 1. The traditional duty-cycled spinning (DCS) algorithm alternates between periods of needle insertion with periods of needle insertion with rotation [6], [7]. Our proposed methods for duty-cycling the steerable needle are bidirectional duty-cycled spinning and duty-cycled flipping.

A. Bidirectional Duty-Cycled Spinning (BDCS)

Similar to prior work, our first control method varies the ratio of pure insertion to insertion *with* rotation to control curvature. However, we alternate the direction of rotation, with a maximum rotation of 360° clockwise or counterclockwise. As with traditional duty-cycled spinning algorithms, while assuming constant insertion and rotation velocities, the duty cycle, D, can be defined as follows:

$$D = \frac{\tau_{\text{rot}}}{T} = \frac{\tau_{\text{rot}}}{\tau_{\text{rot}} + \tau_{\text{trans}}} \tag{1}$$

where T is the duty cycle period, and τ_{rot} and τ_{trans} are the rotation and translation periods, respectively. The resulting curvature of the needle path, κ, is then defined as a function of the maximum needle curvature, $\kappa_{\max}$, and the duty cycle.

$$\kappa = \kappa_{\max}(1 - D) \tag{2}$$

To implement our bidirectional duty-cycled spinning algorithm, we take a slightly different approach than traditional methods to account for alternating rotation. We subdivide an overall desired insertion distance, s, into k substeps of size ds. We choose a constant insertion velocity, u, for each substep based on the rotation period of the rotation motor, t_{rev}. This ensures that at each iteration of our algorithm, the needle tip will return to its prior orientation and will not lead to planar drift over time. During a substep, needle insertion will occur either with or without needle rotation, depending on the duty cycle. Our insertion velocity input, u, and rotation velocity input, ω, are defined for each iteration, $i \in (0,k)$, as follows.

$$u_i(t) = ds/t_{\text{rev}} \tag{3}$$

$$\omega_i(t) = \begin{cases} 2\pi/t_{\text{rev}} & \text{if } iT \geq t < T(i+D), i = 0,2,4\ldots \\ -2\pi/t_{\text{rev}} & \text{if } iT \geq t < T(i+D), i = 1,3,5\ldots \\ 0 & \text{otherwise} \end{cases} \tag{4}$$

B. Duty-Cycled Bevel Flipping (DCF)

The second method consists of inserting the needle in discrete steps and flipping the needle bevel 180° in alternate directions (i.e., bevel left and bevel right) between each insertion to achieve a variable curvature path. The duty cycle, D, for this flipping method can be defined in terms of the time the needle inserts in its flipped orientation, T_{flipped} to its unflipped orientation, $T_{\text{unflipped}}$.

$$D = 1 - \frac{T_{\text{flipped}} - T_{\text{unflipped}}}{T_{\text{flipped}} + T_{\text{unflipped}}} \tag{5}$$

The resulting curvature of the needle path, κ, is defined as in (2). To implement the duty-cycled flipping method, we assume a constant insertion velocity, u, and subdivide the total desired insertion distance, s, into k discrete steps, ds. The time it takes for the needle to insert a distance equal to ds is the duty-cycled period, T. Thus, the time for needle insertion in the flipped state would be: $T_{\text{flipped}} = TD$. During flipping and unflipping, insertion is halted to prevent planar deviation and reduce possible tissue damage. Tissue damage could occur during a needle flip; however, the nature of the damage would likely be a small localized cut, as opposed to the continuous coring damage that would occur from duty-cycled spinning. To eliminate the effects of torsional lag and asymmetric lateral forces on the needle during insertion, the direction of needle flip alternates every two duty-cycled periods between clockwise and counterclockwise.

III. Experimental Methods

The purpose of these experiments was to evaluate the three duty-cycling methods for varying the curvature of a custom EM-tracked steerable needle, inserted with a needle steering robot. Evaluation metrics include error between the theoretically ideal needle path, the simulated needle, and the actual needle path, measured from the EM tracker. Force and torque data was also collected during insertion.

A. Needle Steering Robot

The needle steering robot used in these experiments can steer a flexible needle with an asymmetric tip through insertion and rotation of the needle shaft (Fig. 2). A similar robot is described in [2]. Rotation is achieved through a 12 V DC Maxon motor with an encoder. The rotation motor is mounted on a linear stage with a 12 V DC Pittman motor, which provides the insertion degree of freedom for our robot. Computer control of these motors is performed via power amplifier circuits, a National Instruments PCMCIA DAQCard-6024e, and a Lenovo ThinkPad laptop running Ubuntu Linux 9.04. A custom multithreaded C++ application

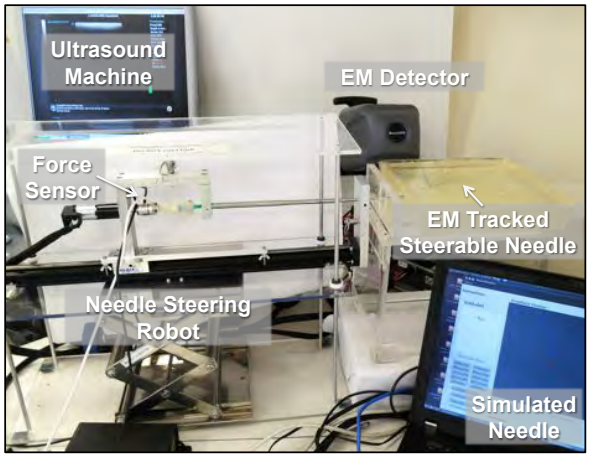

(a) Experimental Setup

(b) Needle Assembly

(c) Needle Components

Fig. 2: The experimental setup with the needle steering robot (a) and and electromagnetically tracked steerable needle (b-c). The components of the steerable needle (c) consist of an electromagnetic tracker, a rotating luer-lock, and hollow pre-bent Nitinol tube with a luer-lock needle hub.

was developed for low-level motor control, execution of the various duty-cycled spinning algorithms, data collection, and simulation of the steerable needle. Insertion and rotation encoders were sampled at 1000 Hz, the low-level motor control loops operated at 500 Hz for the rotational motor (PD control) and 200 Hz for the insertion motor (PID control). The EM tracker and force-torque data were sampled and logged at 100 Hz.

B. Electromagnetically Tracked Steerable Needle

Our custom EM-tracked steerable needle consists of a 41.5 cm long Nitinol tube (0.82 mm OD, 0.50 mm ID) with a pre-bent tip, designed to enclose a custom 6-DOF electromagnetic sensor (41.0 cm long, 0.45 mm OD) designed by Ultrasonix Medical Corporation, partnered with Ascension Technologies, Inc. In clinical practice, the EM tracker could be removed after steering the needle to the desired target, to allow for the introduction of a diagnostic or interventional tool. The pre-bent needle tip was fabricated by inserting a 4 mm long stainless steel solid wire (0.45 mm OD) into the distal end of the needle, securing with adhesive, grinding a 45° bevel as described in [1], and manually bending approximately 4 mm of the distal end of the needle to 30° to create a pre-bent tip. The proximal end of the needle was dipped into a liquid plastic coating to prevent fraying of the tube with repeated use.

The Nitinol needle is attached to the base of the EM tracker via a luer lock system. The needle assembly is held in a custom needle holder that mounts onto the rotational motor of the needle steering robot. CAD models of the needle holder are available on our group's research webpage (http://charm.stanford.edu/Main/Resources). The pose of the EM tracker was sent via TCP/IP from an Ultrasonix SonixMDP ultrasound machine to our custom C++ needle steering program via a Windows-based Ultrasonix data acquisition application and the WINE emulation layer.

C. Simulated and Theoretical Needle Paths

In addition to EM tracked position of the steerable needle tip, we generated (1) a simulated needle path given encoder readings, and (2) an theoretical path based on the theoretical path curvature for each duty cycle. The purpose of the simulated needle path is to evaluate the algorithms without errors due to friction and torsional forces from the phantom tissue, and the purpose of the theoretical path is to compare how closely our algorithms match theoretical predictions.

1) Simulated Needle: For simulation, the needle position and orientation are updated given the insertion and rotation encoder readings using a 3D extension of a method described in our prior work [17]. We assume that (1) the needle tip follows an arc of minimum radius, $r_{\min}$, for a fixed tip orientation, (2) the needle orientation is controlled by rotations about the base of the needle, and (3) the needle shaft follows the tip path. We describe the position and orientation of the needle tip in a reference frame, N, with respect to a starting reference frame for the needle, S, using a 3×3 matrix $g_{sn}(t) \in SE(3)$ [20], [21]. $R_{sn}(t)$ describes a rotation between S and N at time t, and $p_{sn}(t)$ is the position of the needle tip relative to the starting reference frame, S.

A simplified version of the needle kinematic model presented in [5], without angular needle velocity, can be used as an expression for the needle tip configuration. The relative change in needle orientation, as measured by the rotation encoder, can be represented by g_{rot} which describes a rotation about the needle axis, $\vec{e}_2$, by angle θ (between 0° and 360°). Combining the change in needle orientation with the change in insertion distance, ds, as measured by the insertion encoder, allows for computation of the new needle configuration, where $g_{sn}(0)$ denotes the previous needle configuration.

$$g_{sn}(t) = g_{sn}(0)\, g_{\text{rot}} \exp(t\widehat{V}^n_{sn}) \tag{6}$$

$$g_{\text{rot}} = \begin{bmatrix} R_{e3}(\theta) & \mathbf{0} \\ 0 & 1 \end{bmatrix} \tag{7}$$

$$t\widehat{V}^n_{sn} = \begin{bmatrix} 0 & 0 & ds & ds/r_{\min} & 0 & 0 \end{bmatrix}^T \tag{8}$$

2) Theoretical Needle: The theoretical needle path is a perfectly circular arc with an arc length of 12 cm and a radius of curvature defined by (2). This path was generated in MATLAB as a post-processing step. The path generation function takes the duty cycle, insertion velocity, and time vector corresponding to each experimental needle insertion to generate a time-matched theoretical path for each needle insertion.

D. Estimation of Maximum Needle Curvature

To generate theoretical and simulated needle data described above, the maximum curvature of the steerable

needle with the EM tracker, $\kappa_{\max}$, had to be identified. Curvature depends on needle characteristics (i.e., diameter, stiffness, pre-bend angle, etc.) and tissue characteristics (i.e., coefficient of friction, stiffness, homogeneity etc.) [1], [12]. We inserted the EM tracked needle assembly ten times to a depth of 15 cm in the artificial tissue, ensuring that the needle insertion location was new for each insertion and that the needle did not intersect previous needle tracks. We fit circular arcs to the EM data using least squares. The minimum radius of curvature for the needle, $r_{\min}$, was found to be: $r_{\min} = 1/\kappa_{\max} = 12.67$ cm (SD=0.759 cm). We also measured 10 s of EM data for a stationary needle with the moving robot to characterize the noise present in our system and found it to be 0.4037 mm (SD = 0.2455 mm).

E. Experimental Protocol

The steerable needle was inserted 12 cm into an artificial polyvinyl chloride (PVC) phantom (2:1 ratio of plastic to softener) using one of three duty cycle spinning algorithms: (1) continuous rotation duty-cycled spinning, (2) bidirectional rotation duty-cycled spinning, and (3) duty-cycled flipping. Duty cycles of 0%, 25%, 50%, 75%, and 100% were tested for each algorithm, and each insertion was repeated 5 times for a total of 75 needle insertions. For the bidirectional duty-cycled spinning and duty-cycled flipping cases, needle tip position was measured using the EM tracker, and insertion forces and torques were measured with a 6-axis ATI Nano17 force-torque sensor. For all duty-cycling algorithms, the rotational velocity for each iteration step was approximately 2π rad/s and the insertion velocity was 1 mm/s. The duty cycle step, *ds*, was 0.5 cm for the duty-cycled spinning algorithms and 2 cm for the for the duty-cycle flipping algorithm.

IV. Results and Discussion

The needle paths for all trials, grouped by duty cycle, are shown in Fig. 3. The theoretical curve and simulated needle based on encoder readings are shown for each duty-cycling algorithm. For bidirectional duty-cycled spinning and duty-cycled flipping , the EM needle tip position data is also shown. As the EM tracker was not registered to the robot coordinate frame *a priori*, the data was registered to the simulated needle using a fixed-scale Procrustes analysis [22]. The error magnitude between the simulated and EM needle tip position data, and the theoretical curve for each duty cycle is shown in Fig. 4. We note that the motors and metallic components of the robot seem to have some effect on EM needle tip positions errors when the EM needle tip is close to the robot. The errors present between simulated needle data and the theoretic needle path are related to various algorithmic implementation choices, the analysis of which is beyond the scope of this work.

Examples of insertion force and axial torque magnitude profiles over time for 25% and 100% are shown in Figs. 5 and 6. Though not shown in this paper, we found that as duty-cycle increases, the insertion force for the duty-cycled flipping algorithm looks more similar to the bidirectional

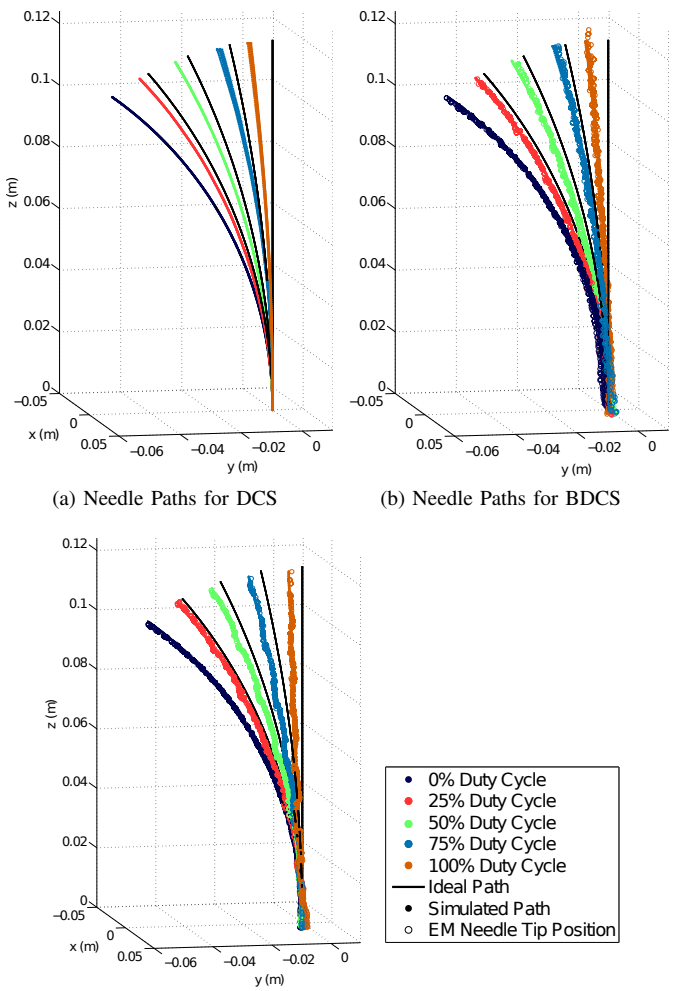

(a) Needle Paths for DCS (b) Needle Paths for BDCS

(c) Needle Paths for DCF

Fig. 3: Simulated needle paths for all duty-cycling methods. For duty-cycled flipping and bidirectional duty-cycled spinning steering algorithms, the needle tip position as recorded with the EM tracker is also shown.

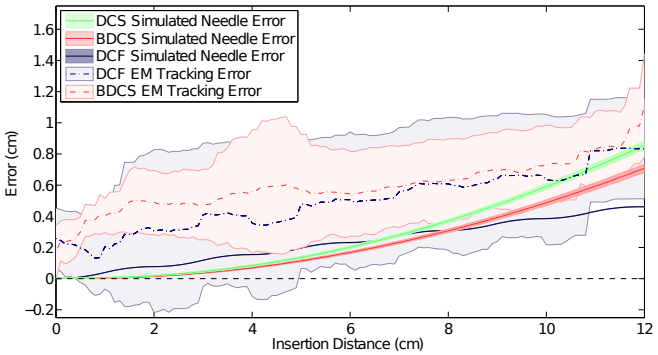

Fig. 4: Example of needle tracking error over time for 100% duty-cycled needle insertions. The mean of 5 needle insertion for each case is shown with the standard deviation. EM tracking data is shown for BDCS and DCF, and the simulated needle error is shown for all algorithms.

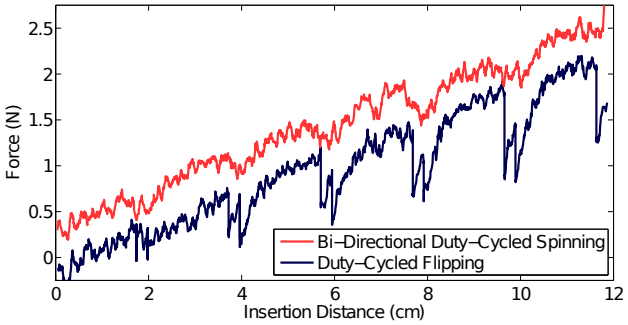

(a) Example Insertion Force for 25% Duty Cycle

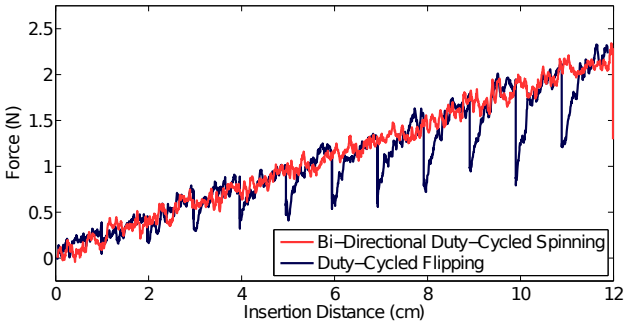

(b) Example Insertion Force for 100% Duty Cycle

Fig. 5: Example insertion force magnitudes for duty cycles of 25% and 100% for BDCS and DCF steering algorithms.

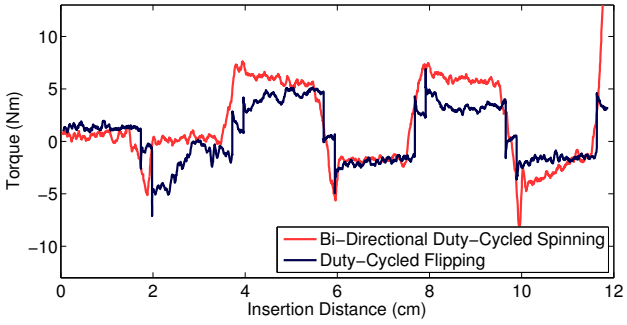

(a) Example Axial Torque Magnitude for 25% Duty Cycle

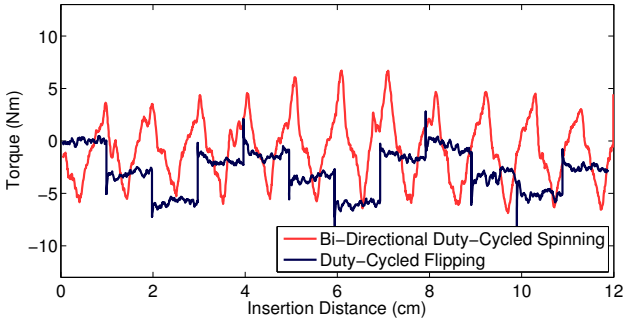

(b) Example Axial Torque Magnitude for 100% Duty Cycle

Fig. 6: Example axial torque magnitudes for duty cycles of 25% and 100% for BDCS and DCF steering algorithms.

rotation duty-cycled spinning. Additionally, for the duty-cycled flipping algorithm, the insertion force has higher variability whereas in the bidirectional rotation case, the axial torque has higher variability. Determining which case, insertion force variability or axial torque variability, has a more significant effect on tissue damage would be an interesting question for future work.

A summary of the insertion force and axial torque magnitudes for needle insertions using duty-cycled flipping and bidirectional rotation duty-cycled spinning are shown in Fig. 7. A single outlier for the 25% duty cycle bidirectional spinning insertions accounts for the large standard deviation. The cause of the spike in insertion force and torque, shown in Figs. 5(a) and 6(a), beginning at approximately 11.5 cm of insertion, is unknown.

An analysis of variance (ANOVA) was used to determine significant differences between groups (i.e., control algorithms and duty cycles) for force and torque data, as well as final end-point error between the EM needle tip position data and the simulated tip position data (Table I). A post-hoc Scheffe test was performed using the ANOVA test statistic to identify significantly different groups. Effect significance is identified for p-values less than 0.05. Significant groups are indicated with parentheses in Table I.

Important results from this analysis are as follows. No significant difference was found on end-point error for either duty cycle or control method, as measured with EM tracker data or simulated needle insertions from motor inputs. Duty-cycled flipping has significantly less mean insertion force and mean axial torque. This result indicates that duty-cycled flipping might be a good choice for implementation of needle steering with biological tissue, as tissue damage might be reduced. The maximum axial torque was significantly higher for 25% duty cycle case than 0% duty cycle case, likely due to a single outlier in the bidirectional duty-cycled spinning needle insertions. Finally, maximum and average axial torque are significantly lower for insertions with 0% duty cycle, likely due to the fact that the needle is not spinning for these cases.

V. CONCLUSIONS

We have demonstrated two novel algorithms for duty-cycled control of robotically-driven steerable needles without the need for continuous rotation. These algorithms could be useful in a variety of needle steering applications where the use of a sensor with a cable is required. We evaluated our algorithms using a custom hollow steerable needle with an embedded electromagnetic tracker and a force-torque sensor. We found no significant differences between the algorithms with regard to end-point error, and significantly lower mean insertion forces and torques for duty-cycled flipping.

An interesting direction for future work could be to explore the relationship between various duty-cycling algorithms and tissue health. Whether insertion force variability or axial torque variability leads to more tissue damage would be an important consideration for the clinical implementation of duty-cycled robotic needle steering. The effect of duty cycle step size on the force and torque profiles would also be an important study for future work.

TABLE I: Statistical Analysis Summary

Source	Control Method (DCS, BDCS, DCF)		Duty Cycle		Interaction
	p	Significant Groups	*p*	Significant Groups	*p*
EM End-Point Error*	0.1123	-	0.4175	-	0.3556
Sim. End-Point Error	0.3416	-	0.0778	-	0.4848
Max. Insertion Force	0.3734	-	0.7291	-	0.0313**
Mean Insertion Force	0.0318	DCF lower	0.3719	-	0.0197
Max. Axial Torque	0.0774	-	0.0147	0% lower than 25%	0.5109
Mean Axial Torque	<0.0001	DCF lower	<0.0001	0% lower than rest	<0.0001

DCS–duty-cycled Spinning, BDCS–Bidirectional duty-cycled Spinning, and DCF– duty-cycled Flipping. Duty Cycle: 0%, 25%, 50%, 75%, 100%.
* This measurement is only evaluated for DCF and BDCS. ** Insignificant main effects shed doubt on the significance of the interaction effect.

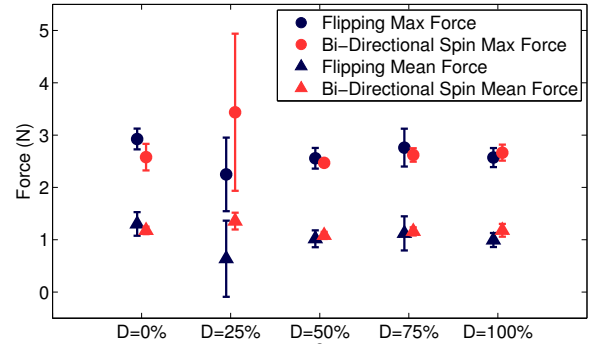

(a) Insertion Force Summary

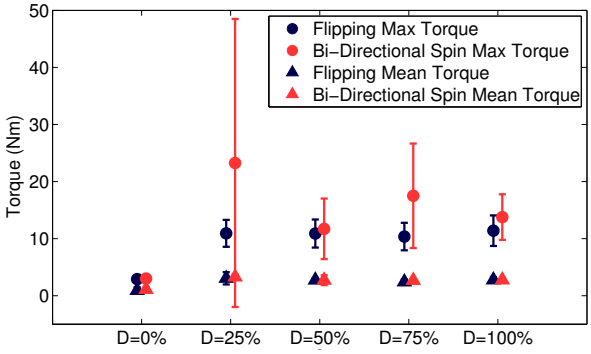

(b) Axial Torque Summary

Fig. 7: Maximum and mean insertion forces and axial torque magnitudes for BDCS and DCF. The mean of the 5 insertions for each condition is shown, with standard deviation error bars. The large error bar for 25% duty cycle bidirectional spinning is due to a single outlier.

The ultimate goal of this work is to implement our duty-cycling algorithms with teleoperated robotic needle steering. Thus, the duty cycle step size and ratios of rotational to insertional velocity used in our algorithms could be further optimized to more closely mimic typical human movement speeds, creating a more natural human-robot interaction.

ACKNOWLEDGMENT

The authors thank Ultrasonix for support on interfacing with the ultrasound machine, and Johnson Matthey for donating materials for the EM needle design.

REFERENCES

[1] A. Majewicz, T. Wedlick, K. B. Reed, and A. M. Okamura, "Evaluation of robotic needle steering in ex vivo tissue," in *Proc. IEEE Int. Conf. Robot. Autom.*, 2010, pp. 2068–2073.

[2] A. Majewicz, *et al.*, "Behavior of tip-steerable needles in ex vivo and in vivo tissue." *IEEE Trans. Biomed. Eng.*, vol. 59, no. 10, pp. 2705–15, 2012.

[3] E. C. Burdette, *et al.*, "The ACUSITT ultrasonic ablator: the first steerable needle with an integrated interventional tool," in *SPIE Medical Imaging*, 2010, p. 7629.

[4] D. Minhas, J. A. Engh, and C. N. Riviere, "Testing of neurosurgical needle steering via duty-cycled spinning in brain tissue in vitro," in *Proc. IEEE Eng. Med. Biol. Soc.*, 2009, pp. 258–261.

[5] R. J. Webster, *et al.*, "Nonholonomic Modeling of Needle Steering," *Int. J. Robot. Res.*, vol. 25, no. 5-6, pp. 509–525, 2006.

[6] D. Minhas, J. Engh, M. Fenske, and C. Riviere, "Modeling of Needle Steering via Duty-Cycled Spinning," in *Proc. IEEE Eng. Med. Biol. Soc. 29th Annu. Int. Conf.*, 2007, pp. 2756–2759.

[7] N. A. Wood, C. A. Lehocky, and C. N. Riviere, "Algorithm for three-dimensional control of needle steering via duty-cycled rotation," in *IEEE Int. Conf. Mech.*, 2013, pp. 237–241.

[8] K. Hauser, R. Alterovitz, and N. Chentanez, "Feedback Control for Steering Needles Through 3D Deformable Tissue Using Helical Paths," in *Robotics: Science and Systems*, 2009.

[9] P. J. Swaney, J. Burgner, H. B. Gilbert, and R. J. Webster, "A flexure-based steerable needle: high curvature with reduced tissue damage." *IEEE Trans. Biomed. Eng.*, vol. 60, no. 4, pp. 906–9, 2013.

[10] M. C. Bernardes, B. V. Adorno, P. Poignet, and G. A. Borges, "Semi-automatic needle steering system with robotic manipulator," in *Proc. IEEE Int. Conf. Robot. Autom.*, 2012, pp. 1595–1600.

[11] N. Wood, K. Shahrour, M. Ost, and C. Riviere, "Needle steering system using duty-cycled rotation for percutaneous kidney access," in *Proc. Int. Conf. IEEE Eng. Med. Biol. Soc*, 2010, pp. 5432–5435.

[12] T. R. Wedlick and A. M. Okamura, "Characterization of robotic needle insertion and rotation in artificial and ex vivo tissues," in *IEEE Int. Conf. on Biomed. Robot. and Biomechatron.*, June 2012, pp. 62–68.

[13] L. Frasson, *et al.*, "Experimental evaluation of a novel steerable probe with a programmable bevel tip inspired by nature," *Journal of Robotic Surgery*, vol. 6, no. 3, pp. 189–197, 2011.

[14] H. Sadjadi, K. Hashtrudi-Zaad, and G. Fichtinger, "Fusion of Electromagnetic Trackers to Improve Needle Deflection Estimation: Simulation Study." *IEEE Trans. Biomed. Eng.*, vol. 60, no. 10, pp. 2706–15, 2013.

[15] S. Patil, J. Burgner, R. J. Webster III, and R. Alterovitz, "Needle Steering in 3D via Rapid Replanning," *IEEE Transactions on Robotics. to appear*.

[16] J. P. Swensen and N. J. Cowan, "An Almost Global Estimator on SO (3) with Measurement on S^2," in *American Control Conference*, 2012, pp. 1780–1786.

[17] A. Majewicz and A. M. Okamura, "Cartesian and joint space teleoperation for nonholonomic steerable needles," in *World Haptics Conf.*, 2013, pp. 395–400.

[18] T. K. Adebar and A. M. Okamura, "3D Segmentation of Curved Needles Using Doppler Ultrasound and Vibration," in *Information Processing in Computer-Assisted Interventions*, 2013, pp. 61–70.

[19] A. A. Geraldes, *et al.*, "On the use of discrete steps in robot-aided flexible needle insertion." in *Proc. IEEE Eng. Med. Biol. Soc.*, 2013, pp. 4867–70.

[20] R. M. Murray, Z. Li, and S. S. Sastry, *A Mathematical Introduction to Robotic Manipulation*. CRC Press, 1994.

[21] V. Duindam, R. Alterovitz, S. Sastry, and K. Goldberg, "Screw-Based Motion Planning for Bevel-Tip Flexible Needles in 3D Environments with Obstacles." in *Proc. IEEE Int. Conf. Robot. Autom.*, 2008, pp. 2483–2488.

[22] J. Gower, "Generalized procrustes analysis," *Psychometrika*, vol. 40, no. 1, pp. 33–51, 1975.